

## Static shift of magnetotelluric data and its removal in a sedimentary basin environment

Alan G. Jones\*

### ABSTRACT

Previous modeling investigations of the static shift of magnetotelluric (MT) apparent resistivity curves have limited appeal in that the electric fields used were point measurements, whereas field observations are of voltage differences. Thus, inhomogeneities of dimension of the order of the electrode line length could not be investigated. In this paper, by using a modeling algorithm that derives point voltages rather than point electric fields, I consider the effect on the MT responses of local near-surface distorting structures, which are both outside of, and inside, the telluric electrode array. I show that static-shift effects are of larger spatial size but of less magnitude than would be expected from conventional modeling. Also, the field observation that static shift affects only the apparent resistivity curve but not the phase response can be replicated by the voltage difference modeling.

If there exists within the earth a layer whose variation in electrical resistivity along the profile can be treated in a parametric fashion, then static shift of the apparent resistivity curves can be corrected. Deriving the modal value from a sufficient number of observations for the layer resistivity is the most useful approach.

### INTRODUCTION

Static shift of magnetotelluric (MT) data is the bane that currently prevents more widespread acceptance and application of the method, not only for problems of academic interest but also for those of a more commercial nature. Static shift of an apparent resistivity curve is caused by an erroneous measurement of the pertinent horizontal component of the earth's electric field of *regional* interest, where the size of the region is given by the appropriate scale length at the period of interest (see below). The erroneous values are due to the potential difference between the electrode pair not truly repre-

senting the horizontal electric field component because of the presence of charges on local surficial, or near-surface, lateral inhomogeneities. The effect is closely related to the current channeling problem of MT data (see, for example, Jones, 1983a); however, it differs from the latter in that even at the highest frequency the potential difference does not give the correct amplitude for the regional electric field, whereas the phase lead of the electric field over the magnetic field is correct. The appropriate scale length at a particular period is either (1) the inductive scale length, which can be taken to be given by either the real part of Schmucker's *C* function (the depth of the maximum eddy current flow, Weidelt, 1972), or by the Niblett-Bostick depth (Niblett and Sayn-Wittgenstein, 1960; Bostick, 1977; Jones, 1983b); or (2) the electrode dipole separation, whichever is the greater. Static shifts of apparent resistivity curves are evident in the published MT literature, particularly in regions where the surficial layer is highly resistive (see, for example, Berdichevsky et al., 1980; Demidova, 1986; Kurtz et al., 1986a,b). Three-dimensional (3-D) numerical modeling studies by Park et al. (1983), Wannamaker et al. (1984), and Park (1985) have shown that 3-D inhomogeneities can radically affect the responses observed, and in particular Wannamaker et al. (1984) emphasize the role played by charges on the boundaries that are ignored, for example, when modeling 3-D data by 1-D or 2-D solutions. These charges are of a more minor consequence in the *B*-polarization, or TM, mode than in the *E*-polarization, or TE, mode of induction, as they are correctly represented on some of the boundaries of the body (see also Jones, 1983a). However, at sufficiently short periods, the modeled apparent resistivities must asymptotically approach the correct value, and accordingly, these modeling studies illustrate current channeling rather than static shift.

The basic difference between current channeling and static shift is that static shift does not affect the phases of the MT impedance tensor, whereas current channeling does. Thus, static shift is, as implied, a shift of the apparent resistivity curve by the same multiplicative factor at all frequencies such that the shape of the curve is retained when plotted on a log-ordinate scale without any corresponding change in the

Manuscript received by the Editor April 14, 1987; revised manuscript received November 5, 1987.

\*Geological Survey of Canada, 1 Observatory Crescent, Ottawa, Ont., Canada K1A 0Y3.

This paper was prepared by an agency of the Canadian government.

phase curve. As will be shown in the section "Modeling Study," this phase curve independence is due to the finite electrode dipole separation.

The static shift tensor  $\mathbf{C}$ , a  $2 \times 2$  real tensor that is frequency-independent, distorts the true MT tensor  $\mathbf{Z}$  to give the observed tensor  $\mathbf{Z}_0$ , viz.,

$$\mathbf{Z}_0 = \mathbf{C}\mathbf{Z}.$$

If  $\mathbf{Z}$  is 1-D, then, as shown by Larsen (1977) and others, it is possible to derive the elements of  $\mathbf{C}$  except for an unknown multiplicative factor ( $D$  in Larsen's nomenclature), and estimates of this factor can be obtained from induction methods that use magnetic fields alone (Larsen, 1977; Fluche, 1983). If  $\mathbf{Z}$  is 2-D, then methods can be used to analyze  $\mathbf{Z}_0$  such that the true regional strike can be determined (Bahr, 1985; Zhang et al., 1987), and after appropriate rotation of the coordinate system, the off-diagonal elements of  $\mathbf{Z}'_0$  (where the prime denotes the rotated impedance tensor) are in error by real multiplicative constants. If  $\mathbf{Z}$  is 3-D, then obviously no decomposition is possible without a priori information. Unpublished studies by Steveling et al., in which  $\mathbf{C}$  is assumed to be a complex  $2 \times 2$  tensor whose elements vary with frequency, have shown that the real parts of the elements are stable, dominant, and frequency-independent, whereas the imaginary parts are relatively much smaller and vary with frequency.

For situations in which  $\mathbf{Z}$  is either 1-D or 2-D, the rotationally invariant impedances are proving useful, and many workers are now adopting and interpreting these. Also, these invariant forms may be validly interpreted in a 1-D manner when the real earth is, in fact, 2-D or even 3-D. There are basically two distinct and different forms, both introduced initially by Berdichevsky and Dmitriev (1976) and termed by them "effective impedances."

The Berdichevsky average is the arithmetic mean of the off-diagonal elements of  $\mathbf{Z}$ , taking the quadrant in which the phase information lies into account, and is given by

$$Z_B = \left( \frac{Z_{xy} - Z_{yx}}{2} \right).$$

This form has been employed by, for example, Ingham and Hutton (1982), Jödicke et al. (1983), Mbipom and Hutton (1983), Ingham (1985), Beamish (1986), Jones and Garland (1986), and Green et al. (1987).

The other form, which is termed the "determinant average" in North American literature and the "effective impedance" in European work, is given by the square root of the determinant of the impedance tensor,

$$Z_D = \sqrt{Z_{xx}Z_{yy} - Z_{xy}Z_{yz}}.$$

It has been used by Berdichevsky et al. (1980), Demidova et al. (1985), Sule and Hutton (1986), and Hutton et al. (1987), and its properties have been discussed by Ranganayaki (1984). For a 2-D earth the determinant average represents the geometric mean of the two off-diagonal impedance tensor elements.

Note that in terms of Eggers's (1982) eigenstate formulation of the MT tensor, for the general case when  $\mathbf{E}^i \cdot \mathbf{H}^i = 0$ , the above defined Berdichevsky and determinant averages are the arithmetic and geometric means of Eggers's eigenvalues  $\lambda^+$  and  $\lambda^-$ , respectively.

The determinant form has the advantage over the Berdichevsky one in that the phase of the determinant  $\phi_D$  is un-

changed by multiplication of the true impedance tensor  $\mathbf{Z}$  by a  $2 \times 2$  real tensor  $\mathbf{C}$  representing static shift, whatever the dimensionality of  $\mathbf{Z}$ . However, there is no reason whatsoever for assuming that any of the other rotationally invariant MT responses, i.e.,  $\rho_B$ ,  $\phi_B$ , and  $\rho_D$ , is any less affected by static shift. Indeed, if only one electrode is close to a local small-scale feature, which may often be the case particularly in sedimentary basins, these averages are inferior to the MT response derived from the unaffected electrode pair. Accordingly, it is emphasized that static-shift corrections should be made to  $\mathbf{Z}_0$  prior to construction of the above invariant forms.

In this paper, I intend to illustrate static shift by 2-D  $B$ -polarization modeling that is based on voltage differences between two locations rather than point electric field values. Results of such modeling, described in detail by Poll et al. (1987), are what we should be comparing our field data to, in that we estimate the electric field from the voltage difference between two electrodes and do not make a point measurement of the field directly. (In contrast, magnetic field measurements are virtually point measurements in space.)

The second part of the paper will describe a technique for removing static shifts from MT data recorded in sedimentary basin environments. Various methods, currently in use for removing static shift, necessitate additional unconventional equipment for their implementation. These include conducting a controlled-source survey in which magnetic fields alone are measured (Andrieux and Wightman, 1984; Sternberg et al., 1985), or deploying many electrode dipole pairs simultaneously [ElectroMagnetic Array Profiling (EMAP) technique, Bostick, 1986; Shoemaker et al., 1986; Word et al., 1986]. However, these methods do not aid in solving the static-shift problem for typical reconnaissance MT surveys or for previously recorded data sets.

What is required is a method that uses the MT responses alone. However, as shown for example by Larsen (1977), when only MT data are available, there always remains an irresolvable static-shift factor. Thus an a priori assumption must be made. One possible method is to derive a regional or global resistivity curve from the profile and to shift the data to match this curve in some manner (e.g., Gordienko et al., 1981; Krasnobayeva et al., 1981; Warner et al., 1983; Vanyan et al., 1983), a procedure which implicitly assumes that the earth is 1-D everywhere with distortions due to local inhomogeneities. Alternatively, one could choose a representative frequency and determine an area-averaged apparent resistivity by weighting surrounding sites using a chosen smoothing window (Berdichevsky et al., 1980; Sternberg et al., 1985). Or, the data from a given region could be averaged at each frequency (e.g., Moroz, 1985). Even more restrictive would be requiring all apparent resistivity curves to pass through a single chosen apparent resistivity value at one frequency. However, all of these procedures will obviously lead to erroneous results if, for example, the layer thicknesses change radically or the resistivity of the surface layer changes along the profile. The technique I propose is less restrictive than any of those given above and is also simple in application. For its valid implementation it is necessary that there exist a layer within the sedimentary or other layered sequence whose electrical resistivity varies laterally in a fashion that can be described adequately by a simple parametric model. I illustrate the method on data recorded across the Williston Basin in Canada, a thick Phanero-

zoic basin of up to 2.5 km of sediments overlying Precambrian basement.

MODELING STUDY

Static shift is due to local surface or near-surface inhomogeneities. Generally, these features are 3-D, but to illustrate the problem of static shift, I consider two very small-scale local 2-D surficial bodies in an otherwise 1-D layered earth (Figure 1). The lateral inhomogeneities are 10 m square and of resistivity  $10 \Omega \cdot m$ , embedded in a layer of  $10^3 \Omega \cdot m$  and thickness 200 m which overlies a more conducting zone of  $10 \Omega \cdot m$  down to 2 km depth. Beneath the conducting zone is a resistive basement of  $10^4 \Omega \cdot m$ . At depth, there are layers of  $10^2 \Omega \cdot m$  and  $1 \Omega \cdot m$  to represent the lower crust-upper mantle and the electrical asthenosphere, respectively. Such a 1-D model is of interest for geologic areas where, for example, thick basalt lavas cover oil-bearing sediments. The resolution of parameters of an equivalent 1-D model was discussed by Ilkiskik and Jones (1984).

In the *E*-polarization mode of induction in a 2-D body, there are no charges generated within the earth, and thus static shift effects are absent. However, in the *B*-polarization mode, charges build up on the boundaries of the inhomogeneities, and the electric field is perturbed from its regional value. (Note that in this case of a true 2-D surficial inhomogeneity, obviously one could avoid the whole problem of static shifts by considering the *E*-polarization results alone.) Conventional modeling of these charges is of limited appeal in that the calculated electric field is derived at a point, whereas measured electric fields are determined from the voltage difference between electrodes. Poll et al. (1987) describe their method for computing voltage differences for a given 2-D model; their code was used to generate the results presented below. The voltage differences could be estimated by numerically integrating the derived electric fields at a sufficient number of surface locations from a conventional *B*-polarization code. However, one would always be uncertain that such a numerical determination had been correctly undertaken across surface locations where the conductivity, and thus the electric field, was discontinuous (e.g., locations -55 m, -45 m, and -5 m in Figure 1). In Poll et al.'s (1987) code, point voltages are derived explicitly; thus, the voltage differences are both

simple to construct and accurate (the calculated voltages were compared against analytical solutions by Poll et al., 1987). The point electric field results were computed using Brewitt-Taylor and Weaver's code (Brewitt-Taylor and Weaver, 1976) with recent corrections (J. T. Weaver, Pers. comm. 1986), a code which was shown to be accurate in both the *B* and the *E*-polarization modes by comparison with an analytical control model (Weaver et al., 1985, 1986).

A comparison of point electric modeling and the voltage difference approach for an electrode pair of 25 m separation for the model in Figure 1 is illustrated in Figure 2 for the three periods of 0.01 s, 1 s, and 100 s. The main results are:

- (1) The effect of the inhomogeneities on the apparent resistivities is of larger spatial size for voltage difference than for point electric. Thus, static-shift effects are seen farther from the inhomogeneity for voltage differences.
- (2) The voltage difference static shift introduces both

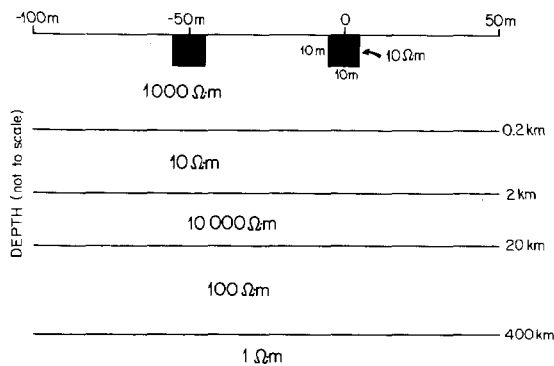


FIG. 1. Two-dimensional model of two small surficial conductive inclusions within a layered earth.

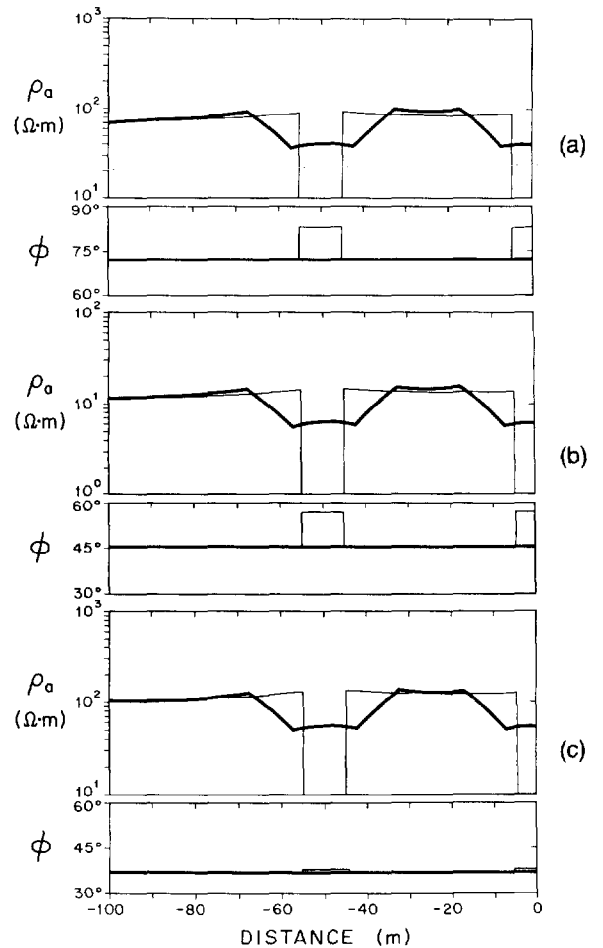


FIG. 2. Conventional point electric field modeling (*fine* lines) compared to voltage difference modeling (*heavy* lines), with an electrode line length of 25 m, for the structure shown in Figure 1 in the *B*-polarization mode of induction at (a) 0.01 s, (b) 1 s, and (c) 100 s periodicity. For the voltage difference modeling, the electrodes are positioned equidistantly about the given distance.

an overestimate and an underestimate of the correct 1-D region apparent resistivity (given by the value at  $-100$  m), and the underestimate is of half an order of magnitude rather than the three or more orders of magnitude determined from the point electric calculations.

(3) Statistically, there is a greater probability of underestimating the true apparent resistivity than of overestimating it. Also, the underestimated value is in error by a greater amount than the overestimated value. (The converse is true for a resistive inhomogeneity, see below.)

(4) The phase derived by the point electric method changes dramatically within the inhomogeneity, whereas the voltage difference phase is exactly the same as the regional value.

Figure 3 illustrates a comparison of the regional 1-D response to the voltage difference responses at locations of  $-70$  m (solid circles) and  $-50$  m (open circles), and static shifts of the voltage difference apparent resistivities by factors of 1.17 and 0.79 with no apparent differences in phase. The phenomenon of shifted apparent resistivities but regionally correct phase values is precisely what is attributed to static shift, but would not have been concluded from the point electric modeling investigation. Also note from Figure 2 that for the point electric modeling as the period increases, the phase deviation from the regional value within the inhomogeneity decreases. Thus, at long periods, point electric modeling gives the regionally correct phase and erroneous apparent resistivity; accordingly, this effect may be attributed to static shift; but, as mentioned in the Introduction, it is actually a current channeling phenomenon.

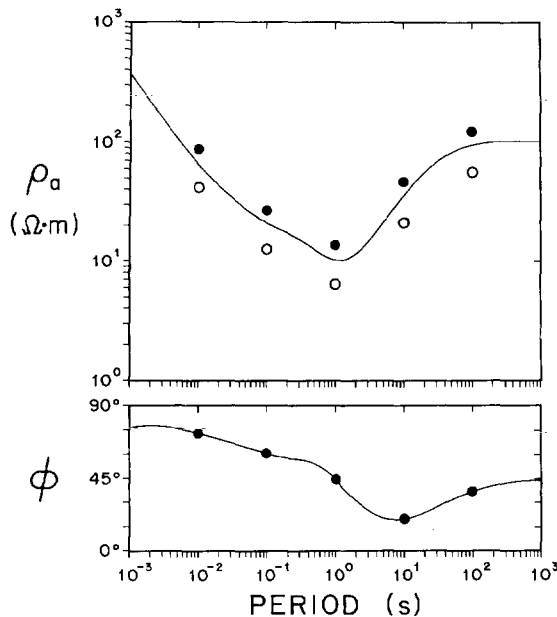


FIG. 3. One-dimensional modeling (solid lines) compared to voltage difference modeling (with 25 m electrode separation) of the structure shown in Figure 1 in the  $B$ -polarization mode of induction at locations of  $-70$  m (solid circles) and  $-50$  m (open circles), i.e., electrodes at distances of  $(-82.5, 57.5)$  and  $(-62.5, 37.5)$ , respectively, for the voltage difference modeling.

Increasing the electrode separation smooths out the static-shift effect, as shown in Figure 4, which illustrates the apparent resistivities that would be observed at 1 s for line length increasing from 25 m to 50 m to 100 m. This feature is the principal phenomenon underlying the Electromagnetic Array Profiling (EMAP) approach (Bostick, 1986; Shoemaker et al., 1986; Word et al., 1986).

If the inhomogeneities are resistive ( $10^5 \Omega \cdot \text{m}$ ) instead of conductive, the results illustrated in Figure 5 for a 25 m dipole at a period of 1 s would be observed. The results for conductive and resistive inhomogeneities are almost reflections of each other about the correct 1-D apparent resistivity of  $10.2 \Omega \cdot \text{m}$ , but in fact the resistive inhomogeneities have a slightly larger multiplicative static-shift factor than do the conductive ones.

This comparison of point electric modeling against voltage difference modeling has important implications for comparing the results of analog to numerical modeling (electrode dipole lengths in analog studies are typically of the order of kilometers to tens of kilometers); or of analog model studies to field data (e.g., Ramaswamy et al., 1980).

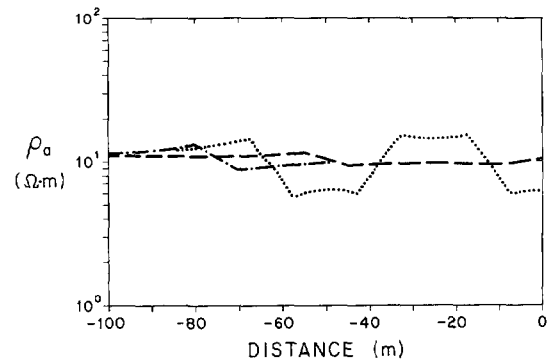


FIG. 4. Effect on the apparent resistivity of varying the electrode line length for the model shown in Figure 1 at a period of 1 s for electrode dipole separations of 25 m (dotted line), 50 m (dashed-dotted line), and 100 m (dashed line).

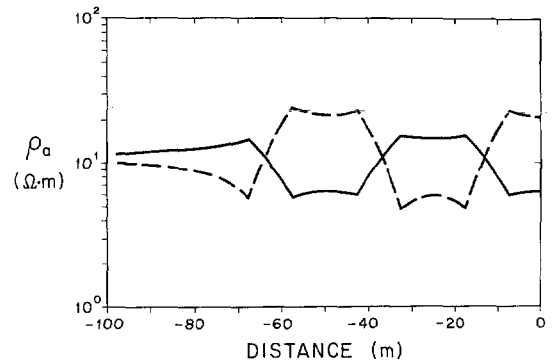


FIG. 5. Conductive (solid line) compared to resistive (dashed line) inhomogeneities at 1 s period for 25 m electric dipole length.

STATIC SHIFT REMOVAL

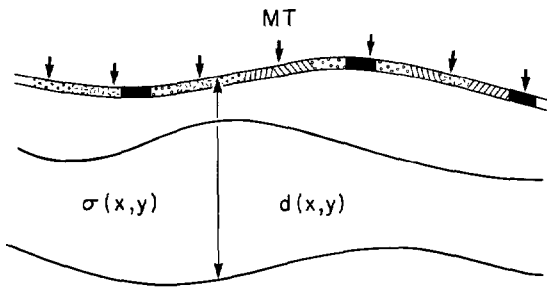


FIG. 6. General model of a highly nonuniform thin sheet above an earth in which a 1-D model is valid up to a maximum period. It is assumed that there exists within the earth a layer whose variation with lateral distance can be described in a parametric fashion, and that estimates of this layer's electrical resistivity are scattered about the locally true value.

Illustrated in Figure 6 is the assumed conceptual model: a random 3-D thin sheet over an earth in which the layer parameters (depth to base  $d_i$  and resistivity  $\rho_i$ ) vary sufficiently slowly laterally that a 1-D interpretation of the static corrected data at each site is valid up to a certain maximum frequency. From the field observations, we can derive for each site and for both polarizations, i.e., both off-diagonal elements of  $Z_0$ , a best-fitting 1-D model appropriate up to a maximum frequency. At each location the true resistivity and depth to the base of the  $i$ th layer are  $\rho_i(x, y)$  and  $d_i(x, y)$ . From the  $Z_{xy}$  response, our estimates of these parameters are given by

$$\rho_{x,i}(x, y) = \rho_i(x, y)D_x^{-2}(x, y)$$

and

$$d_{x,i}(x, y) = d_i(x, y)D_x^{-1}(x, y),$$

(Larsen, 1977) where  $D_x(x, y)$  is the real static-shift factor for that location  $(x, y)$  and for the electric field in the  $x$  direction. We can also obtain an estimate of  $\rho_i(x, y)$  and  $d_i(x, y)$  from the  $Z_{yx}$  responses, viz.,

$$\rho_{y,i}(x, y) = \rho_i(x, y)D_x^{-2}(x, y)$$

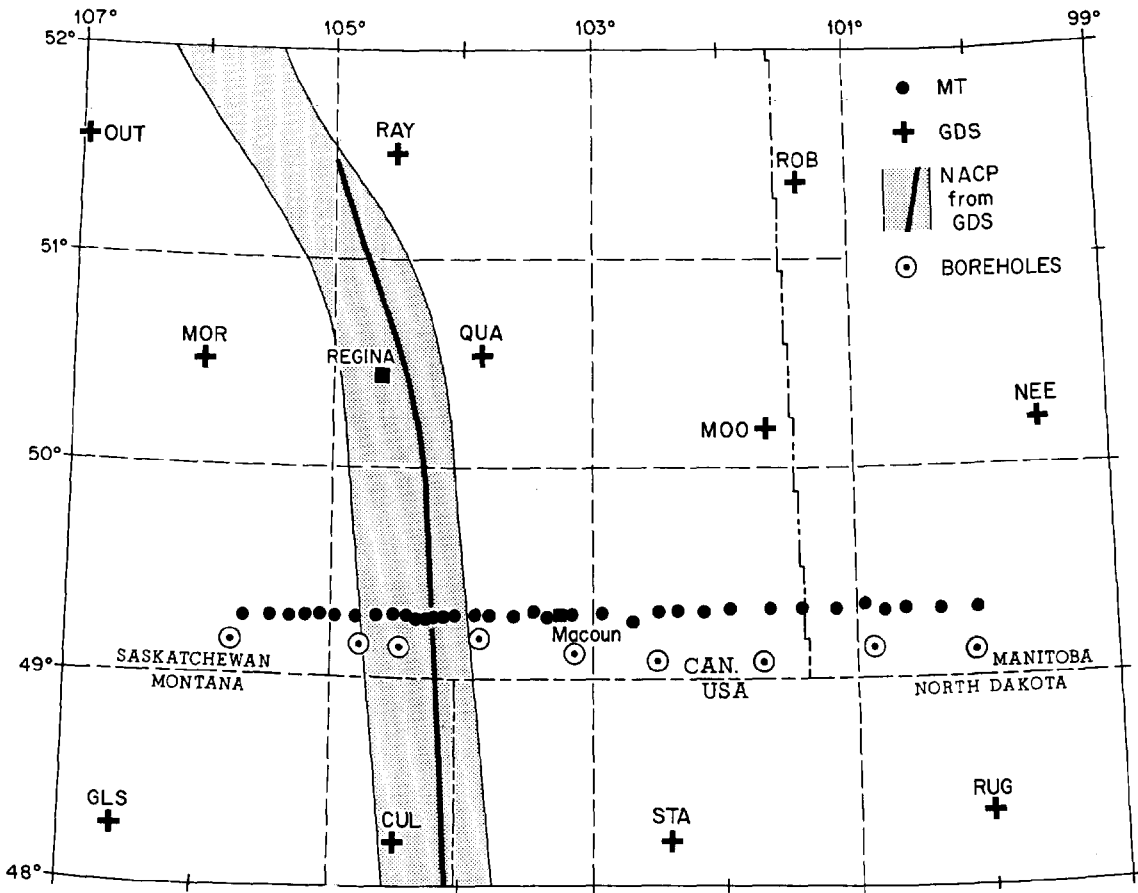


FIG. 7. MT site locations (dots) and boreholes (circled dots). Also shown are the locations of the GDS sites of Alabi et al. (crosses) and their positioning of the NACP anomaly (shaded).

and

$$d_{y,i}(x, y) = d_i(x, y)D_y^{-1}(x, y).$$

There is little cause for  $\rho_i(x, y)$  and  $d_i(x, y)$  to correlate significantly, but  $\rho_{x,i}(x, y)$  and  $d_{x,i}(x, y)$  will correlate because of their interdependence through  $D_x(x, y)$ , and so will  $\rho_{y,i}(x, y)$  and  $d_{y,i}(x, y)$  through  $D_y(x, y)$ . Also, the estimates are all interrelated such that

$$\frac{d_x}{d_y} \sqrt{\frac{\rho_y}{\rho_x}} = 1$$

(dependence on  $x, y$  assumed) must hold.

The method proposed assumes that one of the layers in the sequence, the  $i$ th layer, can be represented in a parametric fashion, and that our estimates of  $\rho_i(x, y)$  given by  $\rho_{x,i}(x, y)$  and  $\rho_{y,i}(x, y)$  vary in some statistical manner about the true value.

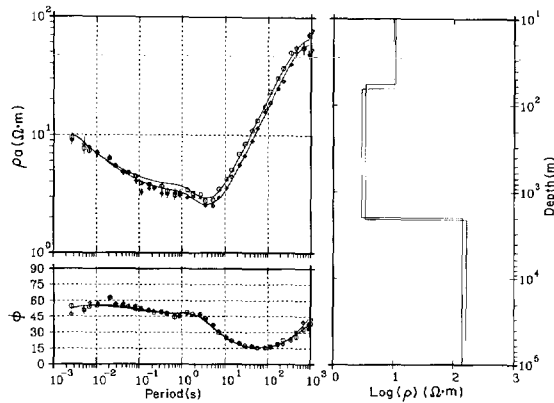


FIG. 8. (Left) MT data from the penultimate westernmost location of the profile (circles are  $x_y$ , or  $E$ -polarization, responses; diamonds are  $y_x$ , or  $B$ -polarization, ones). The two orthogonal data overlap at all periods. The error bars are one standard error, and where bars are omitted, they are smaller than the symbol used to plot the data. The two solid lines are the theoretical responses to the 1-D layered earth models illustrated on the right side.

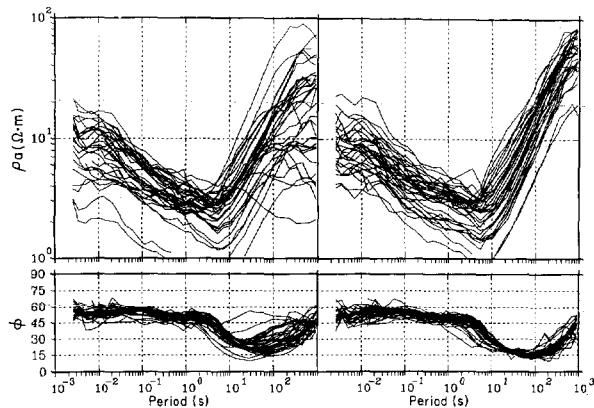


FIG. 9. MT data from all 35 locations along the Williston Basin profile. (a) are the  $E$ -polarization data, and (b) are the  $B$ -polarization data. Note the static shift corruption of the apparent resistivity data.

The data employed to illustrate the technique are from 35 high-quality MT sites along a 407 km east-west profile just north of the U.S.-Canadian border over the Phanerozoic Williston sedimentary basin, which overlies the North American Central Plains (NACP) and the Thompson Belt (TOBE) conductivity anomalies (Jones and Savage, 1986). A geographic site location map, and the positions of the boreholes referred to later, are given in Figure 7, together with the positions of the earlier Geomagnetic Depth Sounding sites of Alabi et al. (1975) and their proposed location of the NACP. For locations on the easternmost and westernmost ends of the profile, the data are 1-D for the whole period range of observations, whereas responses from locations directly above the two conductivity anomalies are 1-D up to approximately 10 s period. An example of typical data from one location, the penultimate westernmost site, is illustrated in Figure 8, together with the 1-D layered earth models that explain the observed responses in the two orthogonal polarizations [derived using

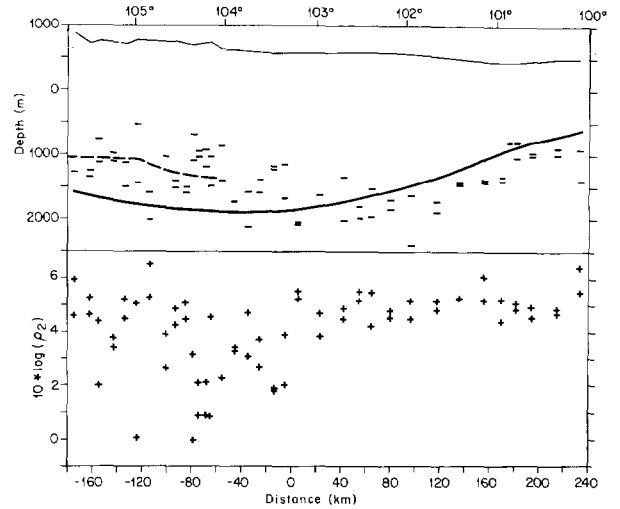


FIG. 10. Derived parameters  $\rho_{x,2}(y)$ ,  $\rho_{y,2}(y)$ ,  $d_{x,2}(y)$  and  $d_{y,2}(y)$  of the second layer from 1-D inversions of the data illustrated in Figure 9. The thick solid line is the mapped position of the Ashern dolomite, the marker horizon between the Upper and Lower Paleozoic sequences; the thick dashed line is the mapped base of the conducting zone in the west of the profile; and the fine solid line is the topography. The longitudinal positions along the profile are indicated by the values west of  $0^\circ$ .

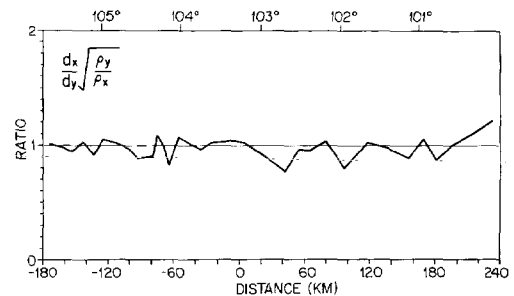


FIG. 11. The ratio  $[d_{x,2}(y)/d_{y,2}(y)] \times [\sqrt{\rho_{y,2}(y)/\rho_{x,2}(y)}]$  for each location along the profile.

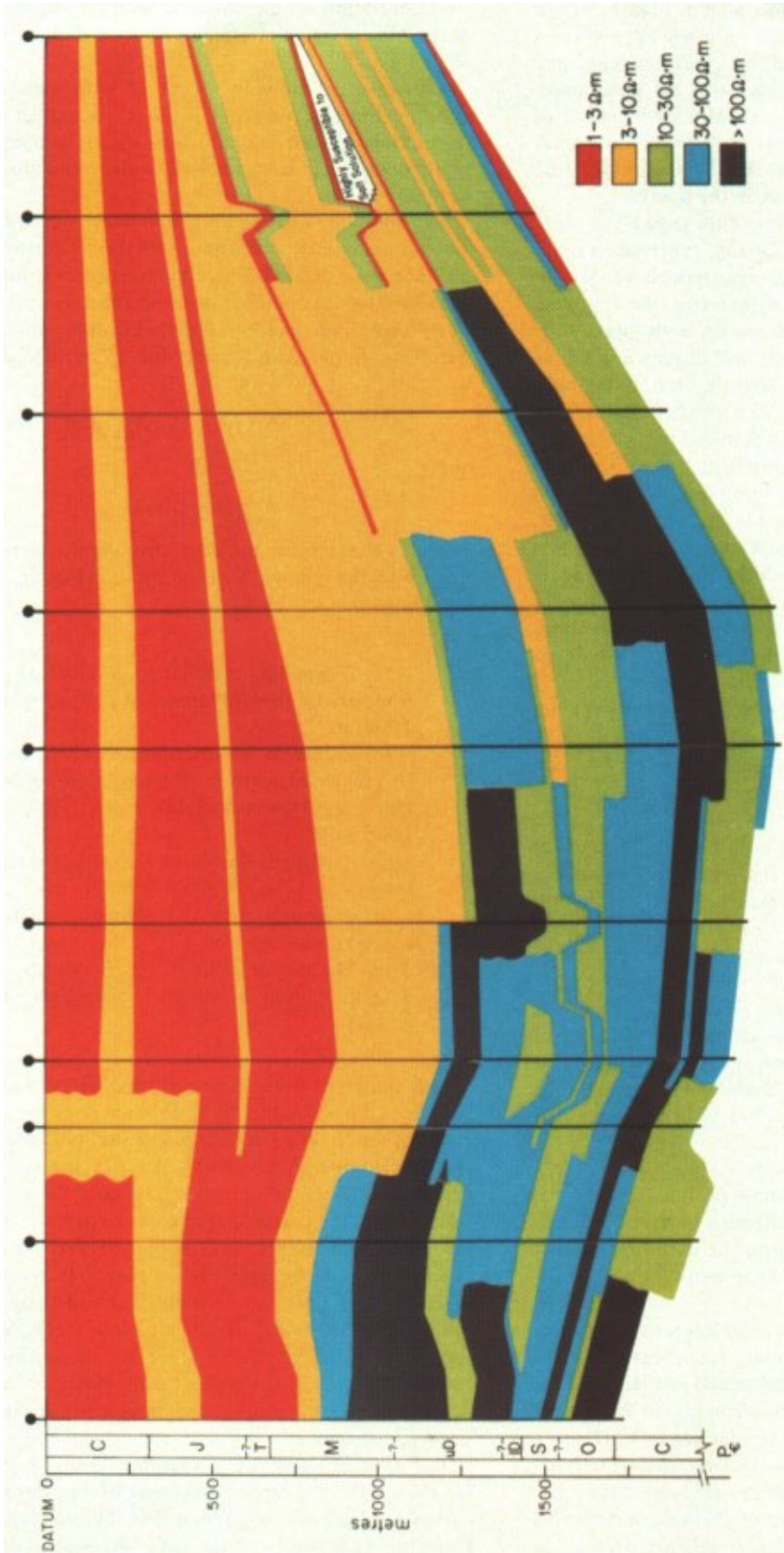


FIG. 12. The electrical Laterolog information from the boreholes along the profile.

Fischer and Le Quang's (1981) MINIM procedure]. The error bars indicate one standard error; where bars are omitted, the standard error is smaller than the symbol used to plot the datum.

The responses from all sites are illustrated in Figures 9a and 9b, where Figure 9a is the  $E$ -polarization mode ( $Z_{yx}$  where  $x$  and  $y$  are geomagnetic north and east, respectively), and Figure 9b is the  $B$ -polarization mode data. No error information is plotted, but generally the estimates have associated standard errors of the order of 1 percent or smaller (see Figure 8 as an example of the quality of the data). Severe static-shift effects of up to one decade are obvious in the figure.

One-dimensional inversions of these data (using the minimization scheme of Fischer and Le Quang, 1981) taken up to 10 s period yielded acceptable three-layer models of type  $H$ , i.e.,  $\rho_1 > \rho_2 < \rho_3$ . We should not expect that the top weathered resistive layer,  $\rho_1(y)$  (dependence on  $x$  dropped since the data are from an east-west profile), will display any simple parametric function with distance laterally, but  $\rho_2(y)$  may. Note that for type  $H$  models,  $S_2$  (the conductance of the second layer  $h_2/\rho_2$ ) is usually the best resolved model parameter, and  $T_2$  (the depth-integrated resistivity  $h_2\rho_2$ ), the least well resolved; the ordering of the resolution of the model parameters obviously depends upon the frequency range (cf., Jones and Foster, 1986). Thus, for imprecise data describing a type  $H$  earth, the resistivity  $\rho_2$  and thickness  $h_2$  are not independently known but only their combination  $S_2$ . For precise data, however, i.e., standard errors of the order of 1 percent, such as the data set analyzed here, both  $\rho_2$  and  $h_2$  are determined to within a standard error of 2 percent.

Figure 10 illustrates the derived second layer resistivities  $\rho_{x,2}(y)$  and  $\rho_{y,2}(y)$ , and depths to base  $d_{x,2}(y)$  and  $d_{y,2}(y)$ , from inversions of the responses illustrated in Figures 9a and 9b. Note that the estimated parameters appear to correlate with the topography at longitudes  $104^\circ$ – $104.5^\circ$  in that there are systematically smaller values for both estimates from sites at this location. Perhaps this correlation is not surprising, since variation in topography often indicates a more inhomogeneous surficial layer. Also shown in Figure 10 is the depth to the top of the Lower Paleozoic sequence, in this region given by the Ashern dolomite marker bed, as derived from well logs coupled with seismic control (Hutt, 1953; Paterson, 1975; Norris et al., 1982; Savage, Pers. comm., 1986).

The correlation coefficients between  $\rho_{x,2}(y)$  and  $d_{x,2}(y)$  and between  $\rho_{y,2}(y)$  and  $d_{y,2}(y)$  are 0.472 and 0.469, respectively, which are statistically significant and well above the expected value for a random correlation of  $1/\sqrt{35} = 0.17$ . Figure 11 illustrates the ratio  $[d_{x,2}(y)/d_{y,2}(y)] \times [\sqrt{\rho_{y,2}(y)/\rho_{x,2}(y)}]$ . The ratio is close to unity for the whole profile. Accordingly, we can be quite confident that the differences between the two orthogonal data at each location, up to the maximum appropriate frequency for validity of the 1-D assumption, are ascribable to static-shift effects.

Figure 12 illustrates the Laterolog electrical resistivity information along the profile for sedimentary sequences below the Second White Speckled shale (a marker bed at the top of the Lower Cretaceous rocks). As is apparent in the figure, the Upper Devonian rocks are far more conductive (3–10  $\Omega \cdot m$ ) in the eastern part of the profile than in the western part (30–100  $\Omega \cdot m$ ). This variation is caused by the Prairie evaporite formation's, which lies conformably on top of the Ashern dolomite, being leached out in the east with highly saline fluid infilling

the porous rock matrix; whereas in the west the evaporite is still dry and the infilling fluid is more resistive. Thus, the MT responses should show the depth of the conducting  $\rho_2$  layer correlating with the Ashern dolomite to the east; but to the west, this depth should correlate with the depth to the middle of the Mississippian strata (shown by a dashed line on Figure 10).

Also of significance in Figure 12 is the small lateral variation in electrical resistivity of the upper part of the Mississippian, Triassic, and Jurassic formations; consequently, these layers collectively conform well to the basic model illustrated in Figure 6.

The  $\rho_{x,2}(y)$  and  $\rho_{y,2}(y)$  estimates were analyzed and various parametric descriptions of their behavior with lateral distance were defined. These parametric descriptions of  $\rho_2(y)$  were used as the basis for deriving the appropriate  $D_x(y)$  and  $D_y(y)$  static-shift factors at each location, and these factors were then employed to correct the  $d_{x,2}(y)$  and  $d_{y,2}(y)$  depths by

$$d_{x,2}^c(y) = D_x(y)d_{x,2}(y)$$

and

$$d_{y,2}^c(y) = D_y(y)d_{y,2}(y).$$

Figure 13 illustrates the corrected depths compared to the depths to the known base of the conducting layer for the following:

- (a) A weighted mean of  $\rho_{x,2}(y)$  and  $\rho_{y,2}(y)$ , weighted inversely by their difference at each  $y$ , resulting in  $\rho_2 = 2.7 \Omega \cdot m$ .
- (b) A second weighted mean, where the  $\rho_{x,2}(y)$  and  $\rho_{y,2}(y)$  estimates were thought to describe three zones given by longitudes  $100^\circ$ – $103.5^\circ$ ,  $103.5^\circ$ – $104.5^\circ$ , and  $104.5^\circ$ – $106^\circ$ .
- (c) A straight-line fit to the  $\rho_{x,2}(y)$  and  $\rho_{y,2}(y)$  estimates.
- (d) A second-order polynomial fit to the  $\rho_{x,2}(y)$  and  $\rho_{y,2}(y)$  estimates.
- (e) The modal value of  $\rho_{x,2}(y)$  and  $\rho_{y,2}(y)$ , which is 3  $\Omega \cdot m$ . Figure 14 shows a histogram of  $\rho_{x,2}(y)$  and  $\rho_{y,2}(y)$ .

It is apparent from Figure 13 that the straight-line fit description of  $\rho_2(y)$  with lateral distance gives the best results in terms of the resulting correlation of the static-corrected depths with the known depths to the base of the conducting layer beneath each location. However, without the a priori well log information, the correct parametric description of  $\rho_2(y)$  would not be known. Hence, it is suggested that the modal value description is to be preferred in that it is a robust statistic, whereas the others can be highly perturbed by outliers. The modal value corrected depths are close to the known depths for most of the profile and are too large, by a factor of  $\sqrt{3.0/2.2} = 1.17$ , at the western end. However, all parametric descriptions give results which are superior to the original uncorrected ones.

The  $\rho_2$  layer resistivity histogram, Figure 14, illustrates that for these data the error introduced by the downward-shifted curves is of greater magnitude than the upward-shifted ones. From the conclusions of the modeling study, we can surmise

that the distorting local inhomogeneities were predominately of higher conductivity than the surrounding host.

The derived static-shift factors  $D_x(y)$  and  $D_y(y)$  from the modal description were then used to correct the observed apparent resistivities to give the static-corrected apparent resistivities

$$\rho_{a,xy}^c(y, T) = D_x(y)^2 \rho_{a,xy}(y, T)$$

and

$$\rho_{a,yx}^c(y, T) = D_y(y)^2 \rho_{a,yx}(y, T)$$

at each period  $T$ . Obviously, an inversion of these static-corrected data will yield a model in which the second layer has a resistivity equal to the adopted modal value of  $3 \Omega \cdot m$ .

The apparent resistivity data prior to, and subsequent to, application of the correction technique are illustrated in Figures 15a, 15b, 15c, and 15d as contoured pseudosections. The uncorrected apparent resistivities (Figures 15a and 15b) show the vertical structure often associated with static-shifted data;

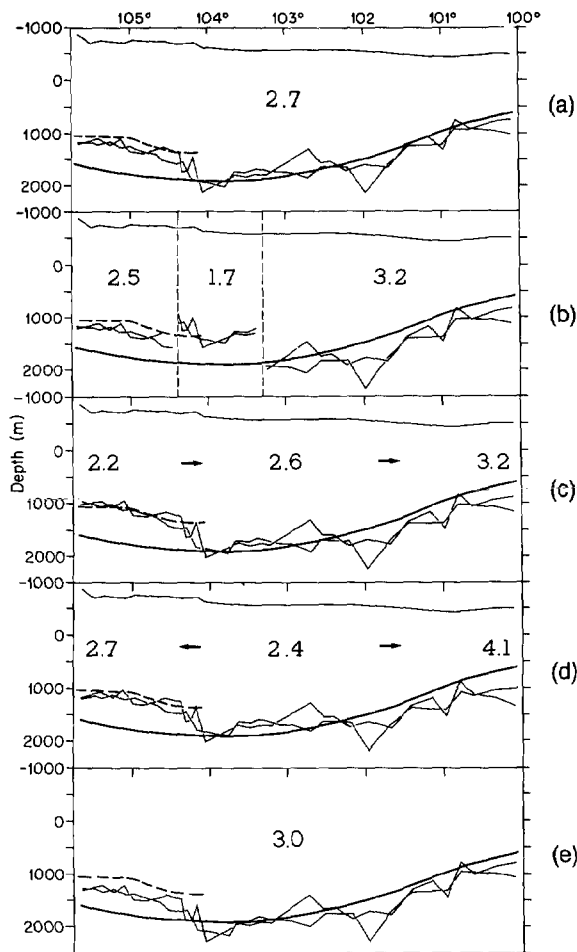


FIG. 13. The static corrected  $d_2$  depths from both the  $\rho_{xy}$  and  $\rho_{yx}$  information, derived for differing parametric descriptions of the second layer with its resistivity being given by the  $\rho_{y,2}(y)$  and  $\rho_{x,2}(y)$  resistivities determined from the data. (a) weighted mean; (b) sectional weighted mean; (c) first-order polynomial fit; (d) second-order polynomial fit; and (e) the modal value. The numbers shown are the second-layer resistivity at that location.

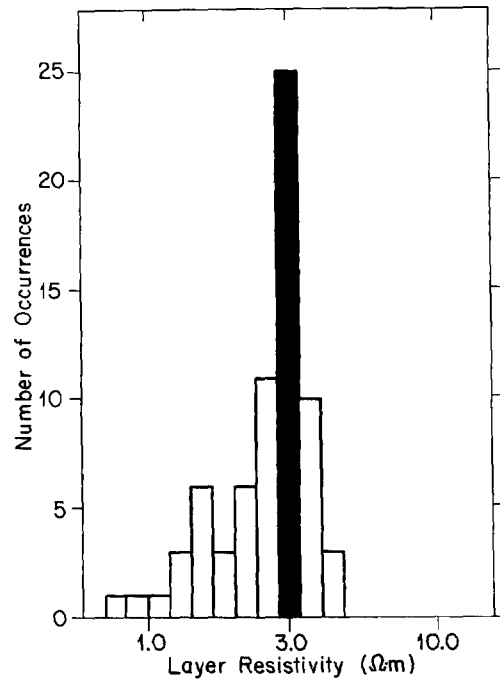


FIG. 14. Histogram of the 70 estimates of  $\rho_2$ .

this is particularly obvious at stations located at positions of 50 km and 120 km. In contrast, the corrected apparent resistivities (Figures 15c and 15d) are much more uniform laterally to periods of 10 s. Note that with this technique the high-frequency asymptotes are permitted to be different, which is necessary because  $\rho_1(y)$  varies radically with distance laterally as the surficial layer becomes more conductive going from west to east. Such variation could not be accommodated using the other schemes described above for static-shift correction based on MT data alone. Figure 16 illustrates all the corrected MT responses, and can be compared directly to the uncorrected ones of Figure 9.

### CONCLUSIONS

I have illustrated static shift of magnetotelluric data by a 2-D theoretical modeling study which takes into account the fact that our field measurements are of voltage differences and not of point electric fields, and have shown that static-shift effects are of larger spatial size but of less magnitude than would be expected from conventional modeling. The empirical phenomenon that phase is unaffected by static shift has been explained.

A method has been proposed for correcting for static shift from data recorded over a region in which one layer may validly be considered to be sufficiently homogeneous laterally that its resistivity can be described as a simple parametric variation with distance. The description considered to be least perturbed by outliers is the modal value of the estimates of the layer's resistivity. An example of the application of this technique to a data set from the Williston Basin in Canada was shown, with a dramatic improvement in the correlation of apparent resistivity curves for each polarization and for neighboring locations evident. Although the method has been illus-

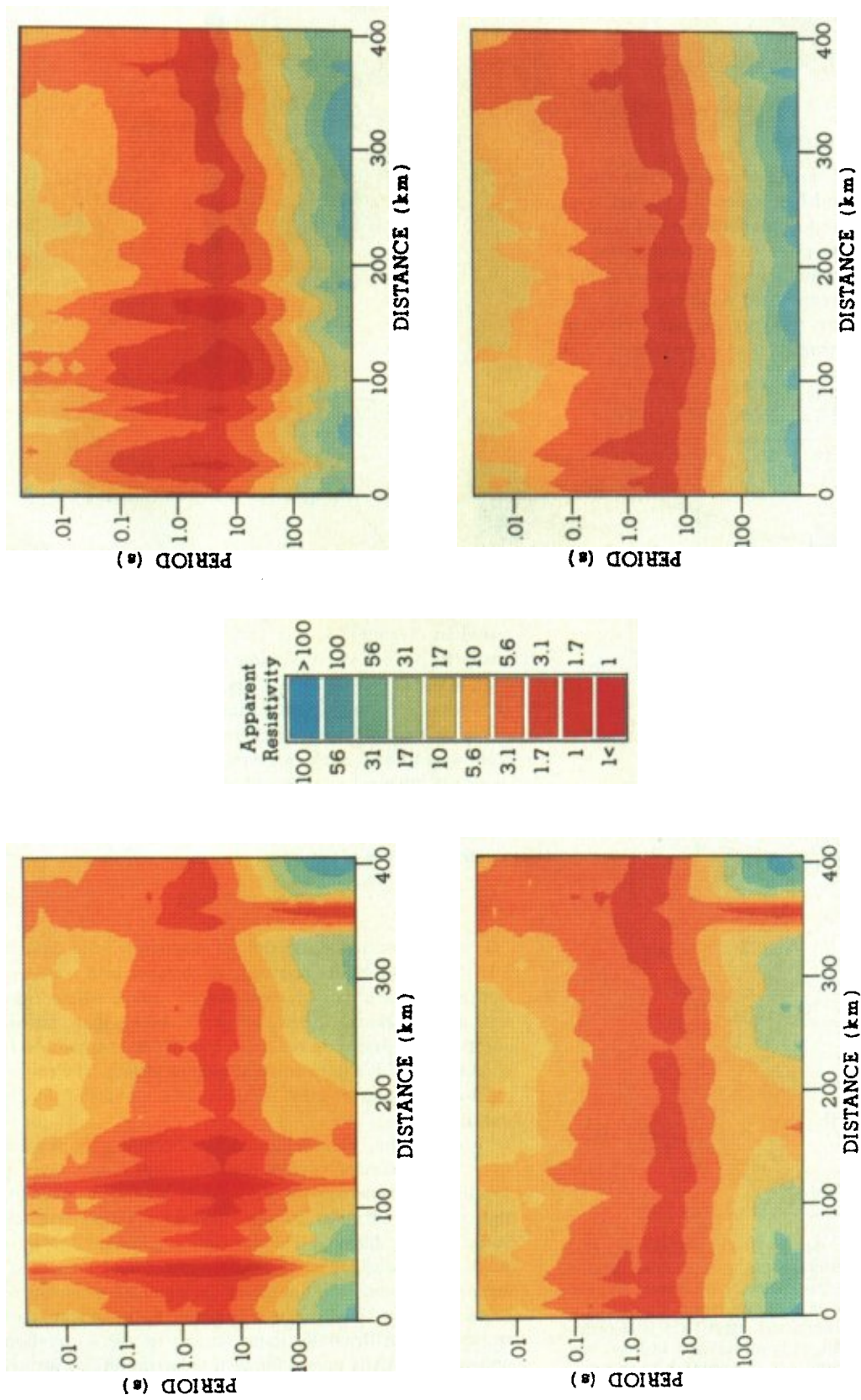


FIG. 15. (a) (top left) The uncorrected apparent resistivities observed in the E-polarization mode of induction plotted as contoured pseudosections. (b) (top right) The uncorrected apparent resistivities observed in the B-polarization mode of induction plotted as contoured pseudosections. (c) (bottom left) The corrected apparent resistivities observed in the E-polarization mode of induction plotted as contoured pseudosections. (d) (bottom right) The corrected apparent resistivities observed in the B-polarization mode of induction plotted as contoured pseudosections.

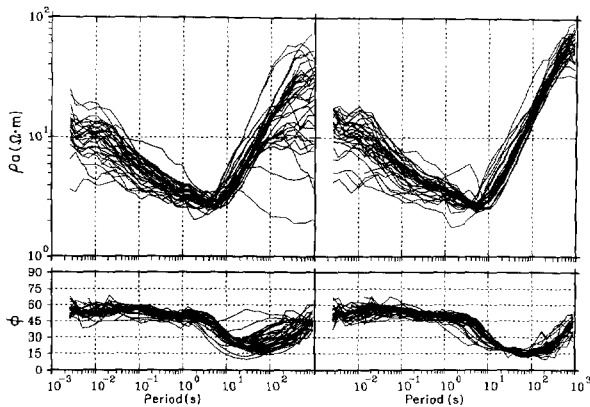


FIG. 16. The static-shift corrected MT data from all 35 locations along the Williston Basin profile. (a) (left side) are the E-polarization data, and (b) (right side) are the B-polarization data.

trated for a sedimentary basin environment, it is also applicable in areas where a layer exists that can be considered to be homogeneous laterally. Such an example is given by Green et al. (1987), where the underplated oceanic layer was assigned a value of  $8000 \Omega \cdot \text{m}$  and inversions of the phase data alone yielded depths to the top of the conducting layer that correlated very well with the depth to the top of a reflecting horizon.

#### ACKNOWLEDGMENTS

I am indebted to Peter Savage and PanCanadian Petroleum Limited of Calgary for providing the data used herein, and to Dr. Gaston Fischer for providing the coding of the minimization scheme described in Fischer and Le Quang (1981). I also wish to thank Professor John Weaver and Helena Poll for discussions and suggestions, and the two referees and the associate editor for their constructive criticism of the submitted version of this manuscript.

Geological Survey of Canada contribution 42386.

#### REFERENCES

- Andrieux, P., and Wightman, W. E., 1984, The so-called static corrections in magnetotelluric measurements: 54th Ann. Internat. Mtg., Soc. Explor. Geophys., Expanded Abstracts, 43–44.
- Bahr, K., 1985, Magnetotellurische Messung des Elektrischen Widerstandes der Erdkruste und des Oberen Mantels in Gebieten mit Lokalen und Regionalen Leitfähigkeits-anomalien: Ph.D. thesis, Univ. of Göttingen.
- Beamish, D., 1986, Geoelectric structural dimensions from magnetotelluric data: Methods of estimation, old and new: *Geophysics*, **51**, 1298–1309.
- Berdichevsky, M. N., and Dmitriev, V. I., 1976, Basic principles of interpretation of magnetotelluric sounding curves, in Ádám, A., Ed., *Geoelectric and geothermal studies*, KAPG Geophysical Monograph, Akadémiai Kiadó, 165–221.
- Berdichevsky, M. N., Vanyan, L. L., Kuznetsov, V. A., Levadny, V. T., Mandelbaum, M. M., Nechaeva, G. P., Okulesky, B. A., Shilovsky, P. P., and Shpak, I. P., 1980, Geoelectric model of the Baikal region: *Phys. Earth Planet. Int.*, **22**, 1–11.
- Bostick, F. X., 1977, A simple almost exact method of MT analysis, in *Workshop on electrical methods in geothermal exploration*: U.S. Geol. Surv., contract no. 14080001-8-359.
- , 1986, Electromagnetic array profiling: 56th Ann. Internat. Mtg., Soc. Explor. Geophys., Expanded Abstracts, 60–61.
- Brewitt-Taylor, C. R., and Weaver, J. T., 1976, On the finite difference solution of two-dimensional induction problems: *Geophys. J. Roy. Astr. Soc.*, **47**, 375–396.

- Demidova, T. A., Yegorov, I. V., and Yanikyan, V. O., 1985, Galvanic distortions of the magnetotelluric field of the Lower Caucasus: *Geomag. Aeron.*, **25**, 391–396.
- Eggers, D. E., 1982, An eigenstate formulation of the magnetotelluric impedance tensor: *Geophysics*, **47**, 1204–1214.
- Fischer, G., and Le Quang, B. V., 1981, Topography and minimization of the standard deviation in one-dimensional magnetotelluric modelling: *Geophys. J. Roy. Astr. Soc.*, **67**, 279–292.
- Fluche, B., 1983, Geomagnetic and magnetotelluric measurements in the 'Hessische Senke': *J. Geomagn. Geoelectr.*, **35**, 693–705.
- Gordienko, V. V., Kulik, S. N., and Logvinov, I. M., 1981, Asthenosphere of Epi-Hercynian platforms: *Geophys. J. (Geofizicheskij Zhurnal)*, **3**, 202–216.
- Green, A. G., Milkereit, B., Mayrand, L., Spencer, C., Kurtz, R. D., and Clowes, R. M., 1987, Lithoprobe seismic reflection profiling across Vancouver Island: *Geophys. J. Roy. Astr. Soc.*, **89**, 85–90.
- Hutt, R. B., 1963, East-West structural cross-section of Saskatchewan: Sask. Govt. Dept. Min. Res.
- Hutton, V. R. S., Gough, D. I., Dawes, G. J. K., and Travassos, J., 1987, Magnetotelluric soundings in the Canadian Rocky Mountains: *Geophys. J. Roy. Astr. Soc.*, **90**, 245–263.
- Ilkisk, O. M., and Jones, A. G., 1984, Statistical evaluation of MT and AMT methods applied to a basalt-covered area in south-eastern Anatolia, Turkey: *Geophys. Prosp.*, **32**, 706–724.
- Ingham, M. R., 1985, Magnetotelluric measurements in the Wellington region: *New Zealand J. Geol. Geophys.*, **28**, 397–404.
- Ingham, M. R., and Hutton, V. R. S., 1982, Crustal and upper mantle electrical conductivity structure in southern Scotland: *Geophys. J. Roy. Astr. Soc.*, **68**, 579–594.
- Jödicke, H., Untiedt, J., Olgemann, W., Schulte, L., and Wagenitz, V., 1983, Electrical conductivity structure of the crust and upper mantle beneath the Rhenish Massif, in Fuchs, K., Ed., *Plateau Uplift*, Springer-Verlag Berlin Heidelberg, 288–302.
- Jones, A. G., 1983a, The problem of "current channelling": a critical review: *Geophys. Surv.*, **6**, 79–122.
- , 1983b, On the equivalence of the "Niblett" and "Bostick" transformations in the magnetotelluric method: *J. Geophys.*, **53**, 72–73.
- Jones, A. G., and Foster, J. H., 1986, An objective real-time data adaptive technique for efficient model resolution improvement in magnetotelluric studies: *Geophysics*, **51**, 90–97.
- Jones, A. G., and Garland, G. D., 1986, Preliminary interpretation of the upper crustal structure beneath Prince Edward Island: *Ann. Geophys.*, **4**, B, 157–164.
- Jones, A. G., and Savage, P. J., 1986, North American central plains conductivity anomaly goes east: *Geophys. Res. Lett.*, **13**, 685–688.
- Krasnobayeva, A. G., D'Yakov, B. P., Astaf'Yev, P. F., Batalova, O. V., Vishnev, V. S., Gavrilo, I. E., Zhuravleva, P. B., and Kirillov, S. K., 1981, Electromagnetic experiments on the Baltic Shield: *Izvestiya, Earth Physics*, **17**, 439–444.
- Kurtz, R. D., DeLaurier, J. M., and Gupta, J. C., 1986a, A magnetotelluric sounding across Vancouver Island sees the subducting Juan de Fuca plate: *Nature*, **321**, 596–599.
- Kurtz, R. D., Ostrowski, J. A., and Niblett, E. R., 1986b, A magnetotelluric survey over the East Bull Lake Gabbro-Anorthosite complex: *J. Geophys. Res.*, **91**, 7403–7416.
- Larsen, J. C., 1977, Removal of local surface conductivity effects from low frequency mantle response curves: *Acta Geodaet., Geophys. et Montanist. Acad. Sci. Hung.*, **12**, 183–186.
- Mbipom, E. W., and Hutton, V. R. S., 1983, Geoelectromagnetic measurements across the Moine Thrust and the Great Glen in northern Scotland: *Geophys. J. Roy. Astr. Soc.*, **74**, 507–524.
- Moroz, Yu. F., 1985, A layer of increased electrical conductivity in the crust and upper mantle under Kamchatka: *Izvestiya, Earth Physics*, **21**, 693–699.
- Niblett, E. R., and Sayn-Wittgenstein, C., 1960, Variation of the electrical conductivity with depth by the magnetotelluric method: *Geophysics*, **25**, 998–1008.
- Norris, A. W., Uyeno, T. T., and McCabe, H. R., 1982, Devonian rocks of the Lake Winnipegosis-Lake Manitoba outcrop belt, Manitoba: *Geol. Surv. Can. Mem.* 392, Manitoba Min. Res. Div. Publ. 771.
- Park, S. K., 1985, Distortion of magnetotelluric sounding curves by three-dimensional structures: *Geophysics*, **50**, 785–797.
- Park, S. K., Orange, A. S., and Madden, T. R., 1983, Effects of three-dimensional structure on magnetotelluric sounding curves: *Geophysics*, **48**, 1402–1405.
- Paterson, D. F., 1975, Computer plotted isopach and structure maps of the Lower Palaeozoic formations in Saskatchewan: Sask. Govt. Dept. Min. Res. Rep. 165.
- Poll, H., Weaver, J. T., and Jones, A. G., 1987, Calculations of voltage differences for magnetotelluric modelling of a region with near-surface inhomogeneities: *Phys. Earth Planet. Int.*, in press.
- Ramaswamy, V., Jones, F. W., Dosso, H. W., and Nienaber, W., 1980,

- A comparison of numerical, analogue model and field-station vertical magnetic fields for the Vancouver Island region: *Phys. Earth Planet. Int.*, **22**, 60–67.
- Ranganayaki, R. P., 1984, An interpretive analysis of magnetotelluric data: *Geophysics*, **49**, 1730–1748.
- Shoemaker, C. L., Shoham, Y., and Hockey, R. L., 1986, Interpretation of natural source electromagnetic array data: 56th Ann. Internat. Mtg., Soc. Explor. Geophys., Expanded Abstracts, 63–65.
- Sternberg, B. K., Washburne, J. C., and Anderson, R. G., 1985, Investigation of MT static shift correction methods: 55th Ann. Internat. Mtg., Soc. Explor. Geophys., Expanded Abstracts, 264–267.
- Sule, P. O., and Hutton, V. R. S., 1986, A broad-band magnetotelluric study in southeastern Scotland. Data acquisition, analysis and one-dimensional modelling: *Ann. Geophys.*, **4**, 145–156.
- Vanyan, L. L., Yegorov, I. V., Shilovsky, P. P., Al'Perovich, I. M., K'Nikiforov, V. M., and Volkova, O. V., 1983, Characteristics of deep electrical conductivity of Northern Sakhalin: *Izvestiya, Earth Physics*, **19**, 208–214.
- Wannamaker, P. E., Hohmann, G. W., and Ward, S. H., 1984, Magnetotelluric responses of three-dimensional bodies in layered earths: *Geophysics*, **49**, 1517–1533.
- Warner, B. N., Bloomquist, M. G., and Griffith, P. G., 1983, Magnetotelluric interpretations based upon new processing and display techniques: 53th Ann. Internat. Mtg., Soc. Explor. Geophys., Expanded Abstracts, 151–154.
- Weaver, J. T., Le Quang, B. V., and Fischer, G., 1985, A comparison of analytical and numerical results for a two-dimensional control model in electromagnetic induction—I. *B*-polarization calculations: *Geophys. J. Roy. Astr. Soc.*, **82**, 263–278.
- 1986, A comparison of analytical and numerical results for a two-dimensional control model in electromagnetic induction—II. *E*-polarization calculations: *Geophys. J. Roy. Astr. Soc.*, **87**, 917–948.
- Weidelt, P., 1972, The inverse problem of geomagnetic induction: *Z. Geophys.*, **38**, 257–289.
- Word, D. R., Goss, R., and Chambers, D. M., 1986, An EMAP case study: 56th Ann. Internat. Mtg., Soc. Explor. Geophys., Expanded Abstracts, 61–63.
- Zhang, P., Roberts, R. G., and Pedersen, L. B., 1987, Magnetotelluric strike rules: *Geophysics*, **52**, 267–278.